Electronic Supplementary Material (ESI) for Lab on a Chip.

A microfluidic double emulsion platform for spatiotemporal control of pH and particle synthesis

Maheen Rana [a], Raheel Ahmad [b], and Annette F. Taylor *[a]

[a] *Department of Chemical and Biological Engineering, University of Sheffield, Sheffield S1 3JD, UK*

[b] *Massachusetts General Hospital Cancer Center and Harvard Medical School, Boston, Massachusetts, 02129, USA*

Supplementary information

Contents

1. Fabrication of the microfluidic device

A thin layer of SU-8 3010 photoresists (MicroChem, Newton, MA) was spin-coated onto a Si wafer and then patterned using ultraviolet exposure through a chrome mask. In the fabrication process, PDMS and the curing agent (SYLGARD 184 Silicone Elastomer) were mixed carefully with ratio 10:1 and decanted onto the patterned SU-8 mold then degassing was performed in a desiccator using vacuum pressure to remove bubbles from the PDMS.

Afterward, the PDMS on Si substrate was baked at 75 °C for 45-50 min. Following the baking, the PDMS was carefully pulled off from the Si substrate, and the microchannels were sliced to suitable sizes. The ports (inlet and outlet) of the PDMS device were punched (0.75 mm rapid core sampling tool, lot No. 161213) and then the microchannel was oxygen plasma-bonded (PDC 002, Harrick Plasma, Ithaca, USA) to the glass slide (24 mm × 60 mm, Menzel Glaser, Germany) for 30 s at 200 W and 200 mTorr. The device was heated in an oven at 75 °C for at least 4 min to anneal the bonding. The widths of the first and second junction were 100 μm and 150 μm, respectively.

2. Surface treatment with PVA

A quick and easy approach to attain hydrophilicity is to treat the PDMS surface with polyvinyl alcohol (PVA) which is a hydrophilic polymer.[1] As PDMS is intrinsically hydrophobic and the continuous phase needed for the double emulsion droplet formation is water, a hydrophilic surface treatment guarantees thorough wetting of the walls when using the aqueous solution. A 1% PVA solution was used to create the OS (second junction) surface hydrophilic.[2-4] First the PVA powder was stirred in distilled water for 40 min at room temperature. Then we gradually increased the temperature on a hot plate (magnetic hotplate stirrer, ADS-HP-S-NT, with precision temperature controller ADS-TC-NT, Asynt) to 100 °C and stirred for another 40 minutes. Then we reduced the temperature to 65 °C and continue stirring for another 2 hours, adding water to compensate for the losses. Immediately after the plasma bonding and annealing of the device, PVA solution was drawn through the OS inlet reservoir using a 1 mL syringe while maintaining the vacuum at the outlet (using a 20 mL syringe), as illustrated in Figure S1. The chip was set aside for 10 min at room temperature and then heated on a hot plate (magnetic hotplate stirrer, ADS-HP-S-NT, with precision temperature controller ADS-TC-NT, Asynt) at 110 °C for 15 min. The chip was then cooled down to room temperature for 15 min. Three repetitive cycles of the above procedure were performed to create multilayer coating for improved surface treatment. The device is then set to use for the synthesis of W/O/W double emulsions and also can be kept for storage at room temperature as the hydrophilic coating persists for longer periods (several months).

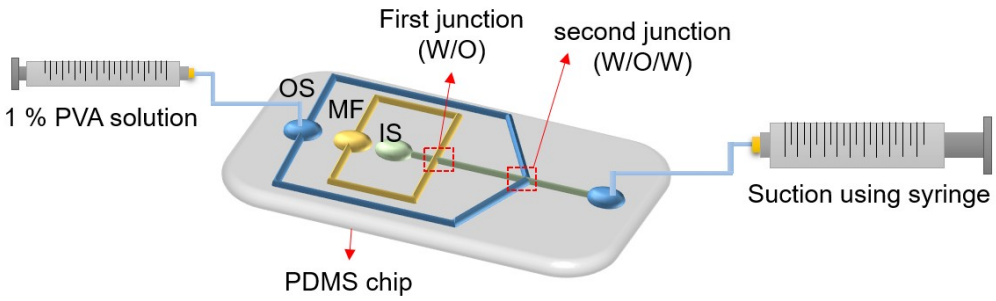

Figure S1. To make the OF (second) junction hydrophilic, following the plasma bonding, 1 % PVA solution (~ 50 µL) was pushed through OF inlet reservoir (using a 1 mL syringe connected via microfluidic-tubing) while applying the negative pressure at the outlet of the device manually using a 20 mL syringe connected through microfluidic-tubing.

3. Set-up for synthesis of the double emulsions

The experimental set-up for the production of the double emulsions is shown in Figure S2. The inner, outer and middle fluids (IS, OS, MF) were driven from the reservoir holding rack connected with the pressure-driven pump (OB1 MkIII+, Elveflow, Paris, France) through microfluidic-tubing (microfluidic fittings 1/32" to 1/16" OD size adapter kit, Darwin microfluidics) to the microchannel. The flow rates were tuned using a custom-built Elveflow Smart Interface (ESI). A 2 mL Eppendorf tube was used as a collection vial for the double emulsions. The process was observed using a phase contrast/epiflouresent microscope connected to a computer.

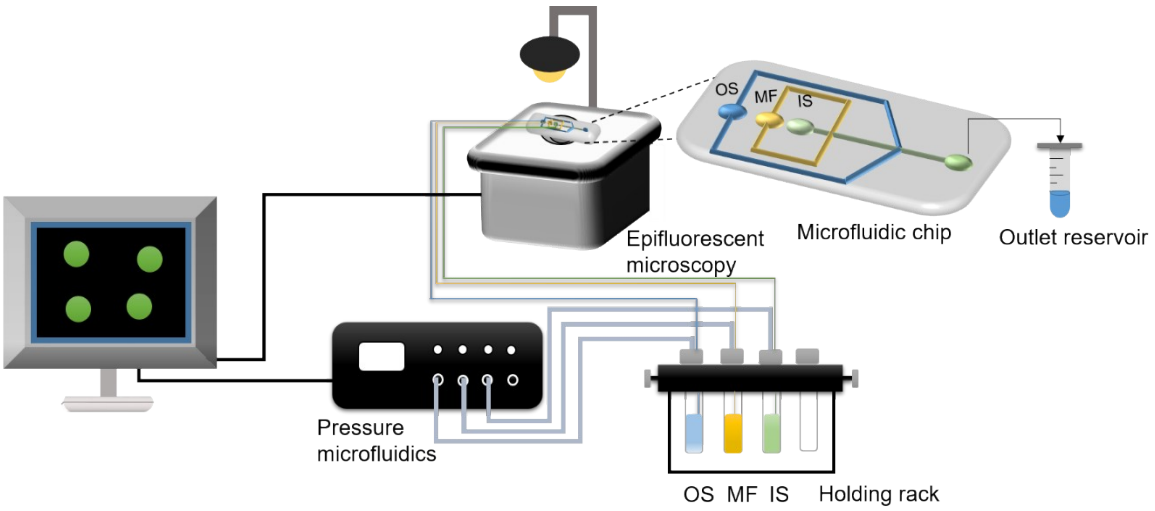

Figure S2. Schematic representation of the experimental procedure for the production of double emulsions. The microfluidic chip was connected to a pressure pump, OB1, and a reservoir holding rack through microfluidic tubing and the process was monitored using optical microscopy.

4. Reaction observation off-chip

The reaction chamber consisted of either CoverWell™ perfusion chambers (8 – 9 mm diameter and 1.2 mm depth) or a chamber constructed in- house (Figure S3). The latter consisted of two pieces of double-sided tape of thickness 100 µm, with a circular hole (1000 µm diameter) produced in each piece of tape using a metal hole punch. The reaction chamber was attached to a microscope slide which was coated to reduce droplet instability and motion. After injection with solution, the chamber was sealed with a glass coverslip and the urea in the external solution diffused into the double emulsion initiating the urease reaction.

For determination of pH, the reaction was monitored in the CoverWell™ perfusion chambers using a Leica TCS SP8 confocal microscope (lens HC PL APO CS2 20x/0.75 DRY or 10x) with 405 nm (intensity: 4 – 8%) and 458 nm laser (intensity: 15 - 30%) consecutively for excitation and the emission wavelength range of 485 – 555 nm (Gain = 600).

The reaction was also monitored in the in-house reaction chambers using an inverted fluorescence microscope to follow the deprotonated form of pyranine (Etaluma LS560 Microscope, green fluorescence, and brightfield, green filter: excitation 457-493 nm; emission 508-552 nm) with the fixed settings of gain = 3.750, illumination = 7.8 %, and exposure = 15.9 using either 4x, 10x, or 20x magnification.

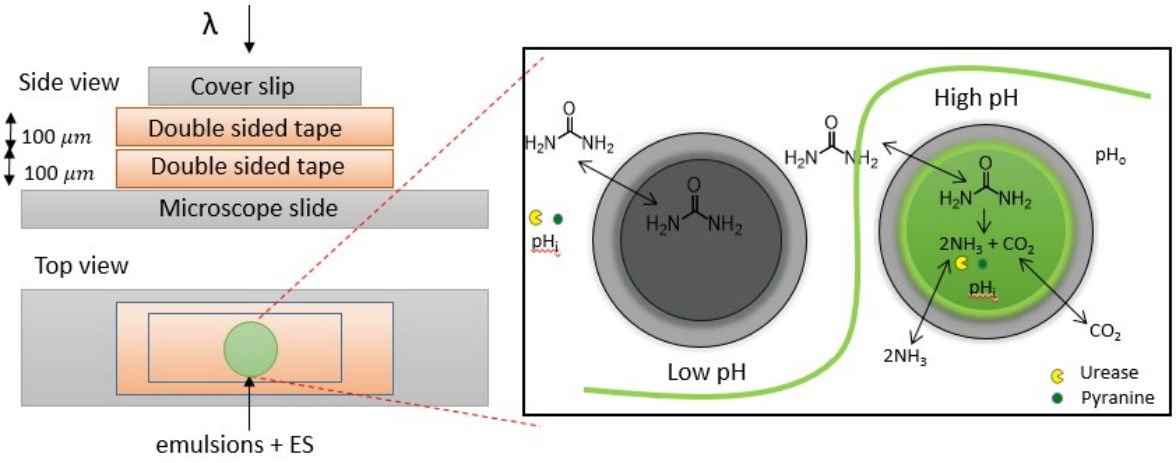

Figure S3. Reaction chamber fabricated in-house from double-sided tape and schematic of process occurring in the emulsion droplets.

5. Calibration of the pH fluoroprobe, pyranine

For determination of the pH, the ratio of fluorescence, R = F_{458}/F_{405}, of pyranine at the two wavelengths is related to the pH through:[5, 6]

$$pH = pKa' - log\left(\frac{R - R_{max}}{R_{min-R}}\right)$$

where R_{min} is the ratio of absorbance of the protonated species ($PyOH^{3-}$), R_{max} is the ratio of absorbance of the deprotonated form (PyO^{4-}) and K_a' is the apparent dissociation constant of pyranine. A solution of a certain pH containing pyranine (50 μM) was prepared using ammonia/ammonium reacted solution with pH adjusted using acetic acid and measured using a pH microelectrode. The solution was injected into a CoverWell™ perfusion chamber and the average intensity of several images was obtained at the two different excitation wavelengths using the confocal microscope. Calibration plots were performed regularly. The standard deviation in intensity was determined to be of order 10%. A fit to the data was obtained in OriginPro using the equation: $y = a + (b - a)/(1 + 10^{(c - x)})$ (Figure S4). The (apparent) pH was determined from SE3: $pH_{app} = c - (1/d)*\log((y - b)/(a - y))$ and, using the formula for the propagation of errors, the error in the pH, s_{pH}, was related to the error in R (s_y): $s_{pH} = (s_y^2((y - b)/(y - a)^2 - 1/(y - a))^2(y - a)^2)/(d^2(y - b)^2))^{1/2}/\ln(10)$.

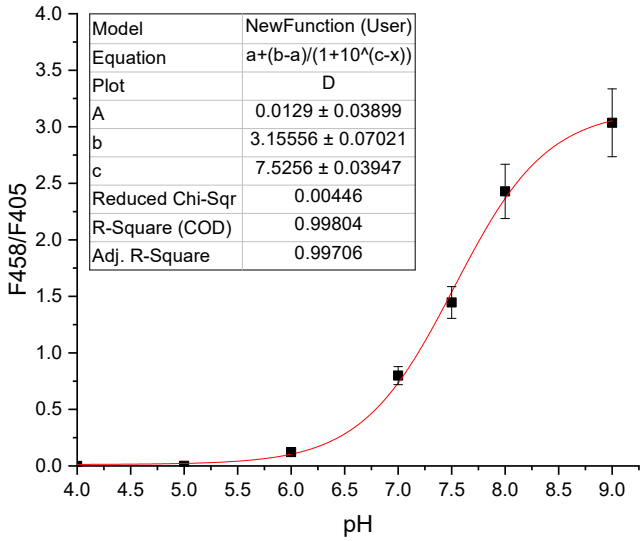

Figure S4. Representative calibration curve for pyranine fluorescence as a function of pH. Average ratio of fluorescence from multiple images (at least 3) obtained using confocal microscopy at λ_{ex} = 450 and λ_{ex} = 405 nm vs pH of solution and fitted equation (line): $y = a + (b - a)/(1 + 10^{d(c-x)})$ where a = 0.013 ± 0.04, b = 3.16 ± 0.07, c = 7.53 ± 0.04. Error bars show 10% standard deviation determined from multiple measurements.

6. Determination of droplet intensity, shell and core sizes

Fluorescent images with λ_{ex} = 405 and 450 nm and the corresponding brightfield images were obtained at regular time intervals with a typical pixel/μm ratio of 111/250. The images were processed using code developed in-house with MATLAB R2020a. The droplets were identified using the λ_{405} image, green channel, (Figure S5A) and a circle constructed around the core using "imfindcircles". The average intensity in the droplets was obtained as the sum of the pixel intensities over the total number of pixels from the images at both λ_{405} and λ_{450}. The ratio of intensities (F450/F405) was then determined and used to find pH (Figure S4). The shell and core size of the droplet was obtained using the brightfield image (Figure S5B and C). The MATLAB code was used to track droplets that were moving and the droplet number was recorded on each image to identify any erroneous measurements.

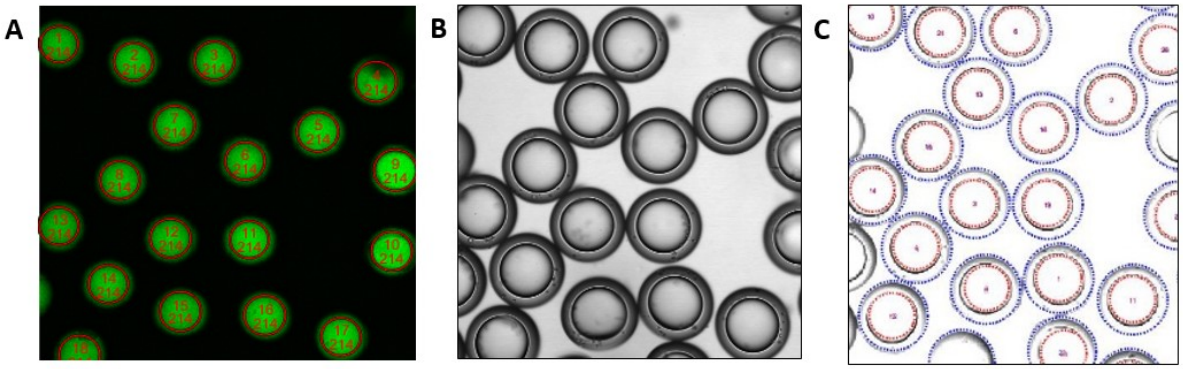

Figure S5. Images obtained of the double emulsion droplets using the Leica confocal microscope and analysis in MATLAB (A) fluorescence image at λ_{ex} = 405 with droplets identified and numbered. The image number (214) is also shown. (B) corresponding brightfield image, (C) core, C, and outer shell, S, identified and used to determine droplet diameter and S/C.

7. Fluorescent labelling of enzyme and determination of concentration

The enzyme was fluorescently labelled following the manufacturer's instructions with some minor modifications (AnaTag™ HiLyte™ Fluor 488 Microscale Protein Labelling Kit). Briefly, a stock solution of 350 U/ml urease (type III) in 1 mM acetic acid was prepared. The urease solution was mixed with the dye solution and then purified. The absorbances at 280 nm and 499 nm were determined using a GENESYS 150 UV-vis spectrophotometer. The absorbance at 280 nm was determined as 0.303 ± 0.006 and at 499 nm as 0.483 ± 0.006 from the average of three independent measurements. The protein concentration was determined from: [protein] = ((A_{280} – 0.19 x A_{499})) x dilution factor/$\varepsilon_{protein}$ where ε = 203000 cm^{-1} M^{-1}, the dilution factor was 1 and hence for a 350 U/ml stock solution, [protein] = 1.04 ± 0.02 μM.

8. Urease reaction in bulk solution

The batch reaction of urease with urea was performed in a 3 mL quartz cuvette with a cross-shaped magnetic stirrer bar. Two stock solutions were prepared; solution A contained urease type III (100 U/mL) in 1 mM acetic acid and solution B contained urea (0.14 M) in 1 mM acetic acid solution. Then 1.4 mL of solution A was added to 1.4 mL of solution B and pH was monitored using a pH microelectrode and DrDAQ pH logger (Figure S6A). The rate of reaction is given by a modified Michaelis-Menten expression:

$$v_0 = \frac{k_1[E]_T[U]}{(K_M + [U])\left(1 + \frac{K_{es2}}{[H^+]} + \frac{[H^+]}{K_{es1}}\right)}$$

where k_1 is the rate constant for decomposition of the enzyme-substrate complex, $[E]_T$ is the concentration of enzyme, $[U]$ is the concentration of urea, K_M is the Michaelis constant, $[H^+]$ is the concentration of acid, and K_{es2} and K_{es1} are the protonation equilibria of the substrate-enzyme complex that give rise to the bell-shaped rate-pH curve. The pH-dependent relationship: rate = $1/(1 + H^+/K_{es1} + K_{es2}/H^+)$ is plotted in Figure S6B with the experimentally determined values of $K_{es1} = 3 \times 10^{-7}$ and $K_{es2} = 1 \times 10^{-10}$.[7]

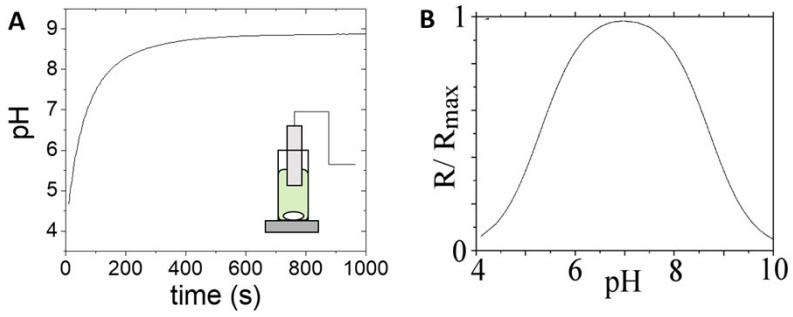

Figure S6. (A) pH time profile in well stirred batch reactor concentrations [urea] = 0.07 M, [acetic acid] = 2 mM; [urease] = 50 Units/mL, [pyranine] = 50 μM, $[\text{phosphate}]_T$ = 80 mM and (B) bell-shaped rate-pH curve produced from theoretical relationship with experimentally determined values of K_{es1} and K_{es2}.

9. Fluorescence in the external solution

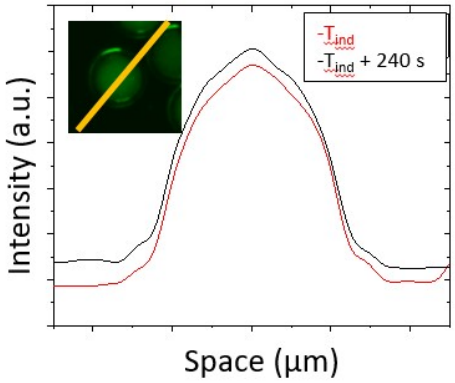

Figure S7. Fluorescence profile across a droplet in chamber with layer depth 200 µM along the indicated line at the induction time, T_{ind}, and at T_{ind} + 240 s showing increase in fluorescence in solution with pyranine included in the external solution. Concentrations were [urea] = 0.07 M, [acetic acid] = 1 mM; [urease] = 50 Units/mL, [pyranine] = 50 µM, $[phosphate]_T$ = 80 mM. + 50 µM pyranine in external solution.

10. Droplet stability

A concentration of 0.28% (w/v) PF-127 was used to stabilize the inner droplet, which is below the critical micelle concentration (CMC) of PF-127 (0.35% (w/v)). With no surfactant we obtained complete dewetting of the inner droplet from the oil (Figure S8(Ai)) and reduced concentration of this surfactant led to partial dewetting (Figure S8Aii). In the absence of reaction, droplets were stable over the course of 48 hours (provided they were not stored in outer solution containing glycerol). In Figure S8B, the % of encapsulated inner droplets is shown at different time points relative to the initial % of double emulsions produced. The inner solution was composed of PF-127 0.28%, and sucrose (0.2 M), with added components: 1 mM acetic acid (orange), 1 mM acetic acid and urea (0.15 M), and 1 mM ammonia solution; the external solution was the same as the inner solution. There was a small loss of the double emulsions over time (determined by the fraction of intact double emulsions compared to total droplets), but there was little difference between the three cases, within experimental error. The S/C was 0.21 – 0.24 in these examples. We also compared stability of droplets with different shell thicknesses; with S/C of 0.17 the droplets were less stable, and dewetting was observed (Figure S8C). The indicated standard deviations were calculated from images of 2 – 4 separate samples. In the double emulsions with reaction, some of the droplets were found to be unstable and this was more prevalent in emulsions with thinner shells (Figure S9A and S9B). Droplets that underwent partial dewetting were observed to react faster than ones that remained stable (Figure S9D and Figure S9E).

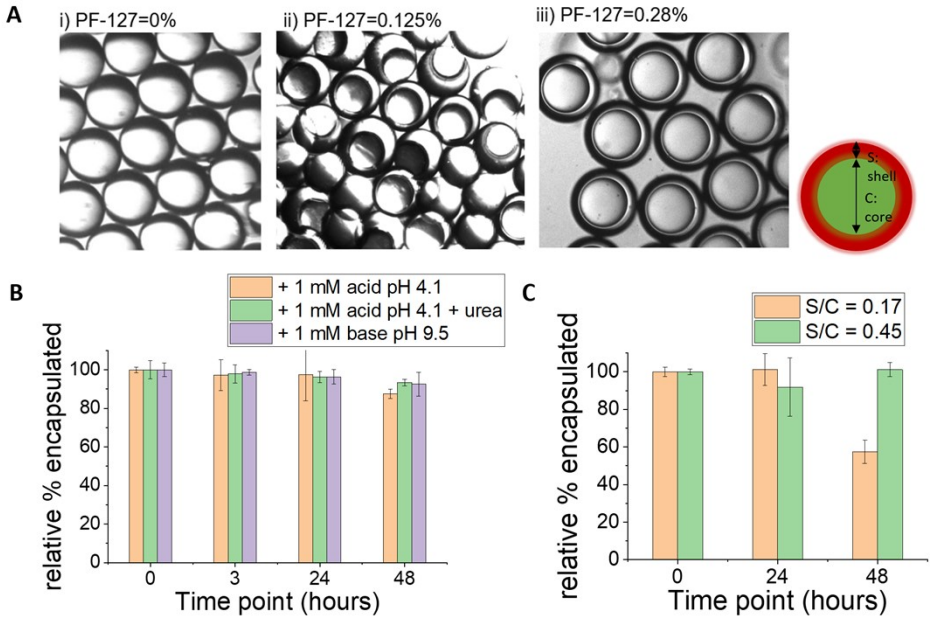

Figure S8. Droplet stability without reaction. (A) Role of PF-127 surfactant concentration in droplet stability (i) complete dewetting with no PF-127; (ii) partial dewetting (iii) stable droplet. (B) Droplet stability (fraction of cores encapsulated compared to initial fraction of intact droplets, S/C = 0.22) over 48 hours with different inner solution (IS) compositions (IS: PF-127 0.28%, sucrose (0.2 M), and added ingredients indicated; the middle fluid was mineral oil, 2% span and 6.5 mM POPC and ES: same as IS). (C) Droplet stability for two different shell:core ratios.

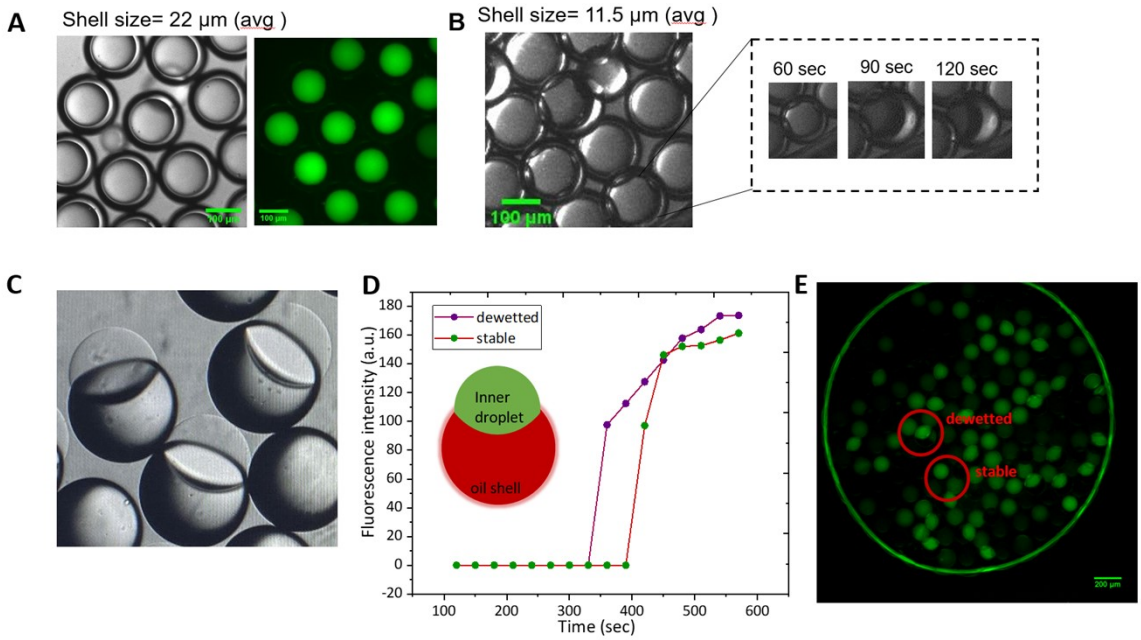

Figure S9. Droplet stability with reaction. (A) Reaction in intact droplets with thick shells (b) Dewetting of droplets with thinner shells during reaction. (C) Image of partially dewetted droplets with core protruding from oil shell. (D) Intensity in time and image of reaction showing that partially dewetted (eye

shape) droplets reacted more quickly than intact droplets (spherical shape). Concentrations were: [urea] = 0.04 M, [pyranine] = 50 μM, [AA] = 2 mM, $[phosphate]_T$ = 80 mM and [urease] = 20 Units/mL.

11. Urease-driven calcium phosphate and calcium carbonate precipitation in bulk solution

The batch reaction of urease with urea was performed in a 3 ml quartz cuvette with a cross-shaped magnetic stirrer bar. Two stock solutions were prepared; solution A contained urease type III (100 U/mL), Phosphate = 0.8 M in 1 mM acetic acid and solution B contained urea (0.14 M) in 1 mM acetic acid solution with 340 mM calcium chloride added. 1.4 mL of solution A was added to 1.4 ml of solution B and pH was monitored using a pH microelectrode and DrDAQ pH logger.

12. Raman Spectra

Calcium phosphate and calcium carbonate crystals were characterized using a Senterra II Raman confocal microscope (Bruker) with an excitation wavelength of 532 nm, and power of 25 mW. The 100x objective was used to obtain images of 1594 x 1192 pixels and resolution of 0.04 μm/pixel. The spectral resolution was 1.5 cm^{-1}. The sample of solution from experiments with bulk solution was air dried on a microscope slide and an image was obtained of the particles with the microscope (Figure S8A). In agreement with earlier work, samples contained a mixture of amorphous calcium phosphate or weakly crystalline hydroxyapatite particles with characteristic Raman peaks at 950 cm^{-1} and larger dumbbell shaped crystals of calcite, with characteristic Raman peaks at 711 cm^{-1} and 1085 cm^{-1} (Figure S10B).[7]

For samples obtained from experiments with the double emulsions, the solution was placed on a microscope slide and spherical particles or microplatelets from burst emulsions were observed. The size of the particles was estimated from the confocal images using MATLAB to be of the order of ~ 500 nm (530 ± 50 nm, Figure S11A). The Raman spectra of the platelets (Figure S11B) contained characteristic peaks at 986 cm^{-1}, 880 cm^{-1} and 585 cm^{-1} of dicalcium phosphate dehydrate, $CaHPO_4 \cdot 2H_2O$, brushite (Figure S11C).[8]

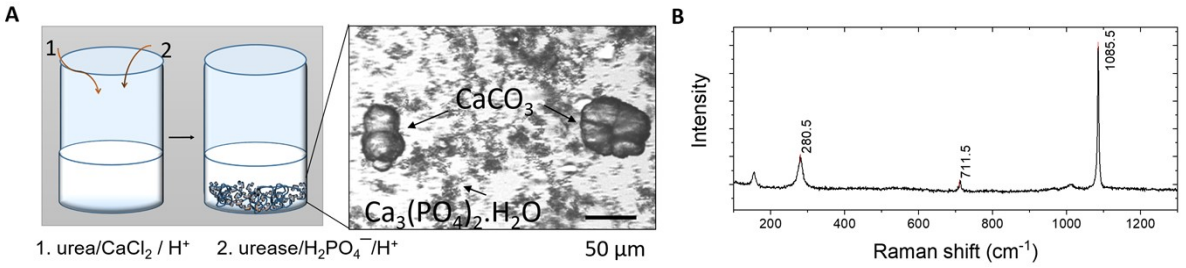

Figure S10. (A) Illustration of batch experiment with production of a mixture of calcium carbonate and calcium phosphate and microscope image of sample. (B) Raman spectra from confocal image of calcium carbonate obtained showing peaks for calcite at 711 and 1086 cm^{-1}.

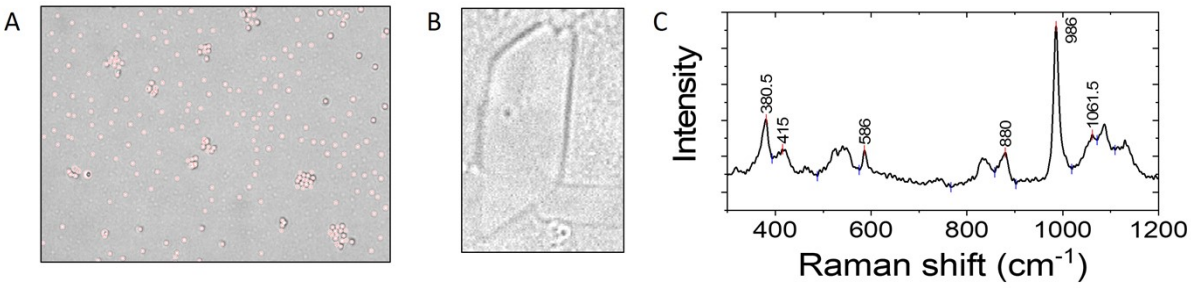

Figure S11. (A) Confocal image (63 x 43 µm) of sample of particles from double emulsion sample and circles obtained using MATLAB for estimating particle size. (B) Confocal image (22 x 32 µm) of sample of platelet from double emulsions. (C) Raman spectrum of platelet obtained from sample showing characteristic peaks for brushite at 986 cm^{-1}, 880 cm^{-1} and 585 cm^{-1}.

13. Determination of apparent area or length of calcium phosphate precipitate

A comparison of the approximate growth rate of the calcium phosphate structures was determined using ImageJ. The green channel of the RGB images obtained using optical microscopy (with resolution 0.75 pixels/µm) was used to find “apparent” area and length since information regarding the 3D structure could not be obtained. The area containing the precipitate was selected. A threshold filter (percentile) was applied giving a binary image with precipitate and the pen tool was used to fill any pixels containing precipitate that were not highlighted (Figure S12A). The area occupied by the precipitate was then extracted. The apparent length of the platelet crystals was obtained from the longest axis and plotted in time from a series of images (Figure S12B). The average growth rate was calculated from the slope of the plot between 600 and 800 s was 0.12 + 0.02 µm s^{-1}.

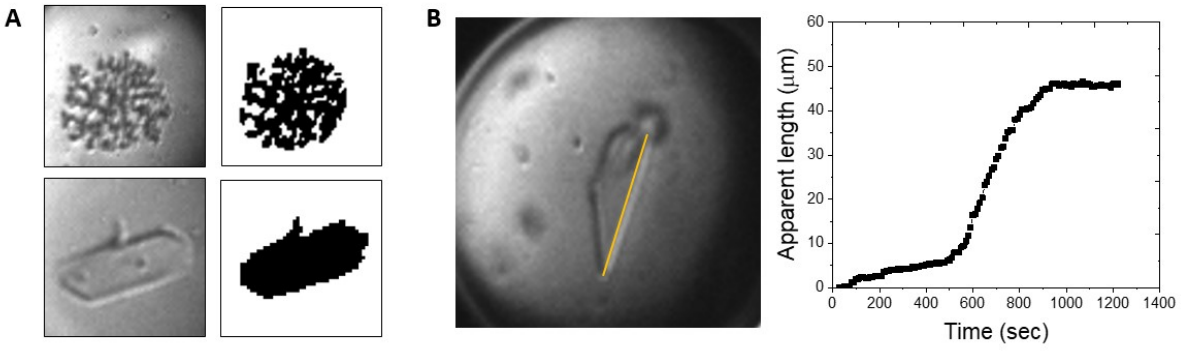

Figure S12. (A) Microscope images of calcium phosphate precipitates (35 x 35 µm) and processed binary images used for determination of apparent area occupied by precipitate. (B) Image of platelet (100 x 100 µm) with longest axis identified (yellow line) and apparent length of the crystal in time.

14. Population level crystals

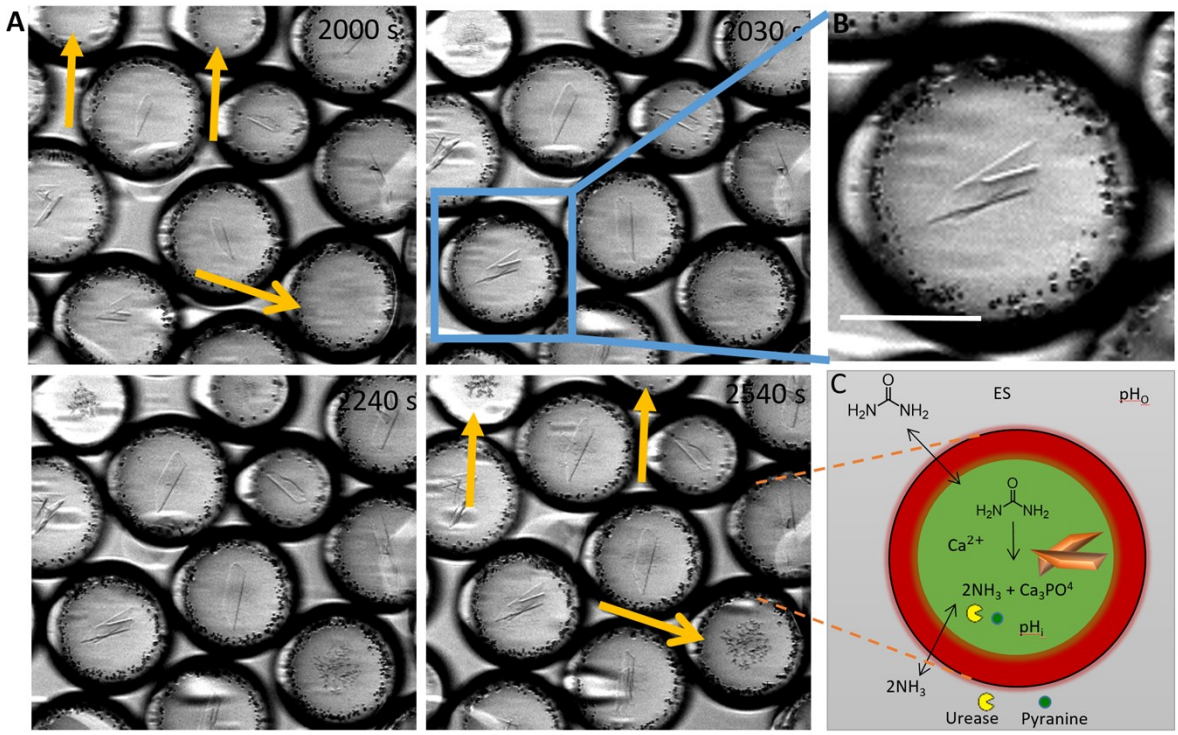

Figure S13. Calcium phosphate formation in a population of droplets with average S/C = 0.09 (the small black circles at the inner oil-water interface are bubbles). The reaction concentrations were: [urea] = 0.15 M, [AA] = 1 mM, [urease] = 50 U/ mL, $[phosphate]_T$ = 80 mM, and $[CaCl_2]$ = 0.15 M (A) Time-lapse imaging of urea-urease triggered precipitate formation. Yellow arrows indicate droplets in which nanoparticles formed. (B) multiple crystals formed in some droplets, brightfield microscope (etaluma, 10x magnification), and scale bar = 50 µm (C) A schematic image of the mechanism of crystal growth triggered by the base production in urea hydrolysis reaction.

References

1. T. Trantidou, Y. Elani, E. Parsons and O. Ces, *Microsystems and Nanoengineering*, 2017, **3**.
2. N. N. Deng, M. Yelleswarapu and W. T. S. Huck, *J. Am. Chem. Soc.*, 2016, **138**, 7584-7591.
3. S. Deshpande, Y. Caspi, A. E. C. Meijering and C. Dekker, *Nature Communications*, 2016, **7**, 1-9.
4. D. Wu, Y. Luo, X. Zhou, Z. Dai and B. Lin, *Electrophoresis*, 2005, **26**, 211-218.
5. R. Bizzarri, C. Arcangeli, D. Arosio, F. Ricci, P. Faraci, F. Cardarelli and F. Beltram, *Biophys. J.*, 2006, **90**, 3300-3314.

6. K. Kano and J. H. Fendler, *Biochimica et Biophysica Acta (BBA) - Biomembranes*, 1978, **509**, 289-299.
7. B. Bohner, T. Bánsági Jr, Á. Tóth, D. Horváth and A. F. Taylor, *Angew. Chem. Int. Ed.*, 2020, **59**, 2823-2828.
8. I. A. Karampas and C. G. Kontoyannis, *Vibrational Spectroscopy*, 2013, **64**, 126-133.